Kohn-Sham potential with discontinuity for band gap materials

M. Kuisma,[1] J. Ojanen,[1] J. Enkovaara,[2] and T. T. Rantala[1]

[1]*Department of Physics, Tampere University of Technology, P.O. Box 692, FI-33101 Tampere, Finland*
[2]*CSC-IT Center for Science Ltd., P.O. Box 405, FI-02101 Espoo, Finland*
(Received 2 March 2010; revised manuscript received 20 May 2010; published 7 September 2010)

We model a Kohn-Sham potential with the discontinuity at integer particle numbers starting from the approximation by (GLLB) Gritsenko *et al.* [Phys. Rev. A **51**, 1944 (1995)]. We evaluate the Kohn-Sham gap and the discontinuity to obtain the quasiparticle gap. This allows us to compare the Kohn-Sham gaps to those obtained by accurate many-body perturbation-theory-based optimized potential methods. In addition, the resulting quasiparticle band gap is compared to experimental gaps. In the GLLB model potential, the exchange-correlation hole is modeled using a generalized gradient approximation (GGA) energy density and the response of the hole-to-density variations is evaluated by using the common-denominator approximation and homogeneous electron-gas-based assumptions. In our modification, we have chosen the PBEsol potential as the GGA to model the exchange hole and add a consistent correlation potential. The method is implemented in the GPAW code, which allows efficient parallelization to study large systems. A fair agreement for Kohn-Sham and the quasiparticle band gaps with semiconductors and other band gap materials is obtained with a potential which is as fast as GGA to calculate.

PACS number(s): 71.15.−m

I. INTRODUCTION

The Kohn-Sham density-functional theory (KS-DFT) (Refs. 1 and 2) with local and semilocal density approximations (LDA and GGA) has proven to be successful in predicting total-energy-related properties of many electron systems, such as crystal structures, molecular geometries and cohesion energies. Therefore, these simple approximations can be used to predict many of the ground-state features of metals, semiconductors, and dielectrics.

Although there is no direct physical interpretation of the KS eigenvalues[3] the eigenvalue differences can be considered as zeroth-order approximations to the excitation energies[4] or the eigenvalues itself as vertical ionization potentials.[5] In some cases, the shape of the valence and conduction bands also resembles the experimentally measured ones, except for the band gap. The physical quasiparticle gap contains, in addition to the KS band gap, the integer derivative discontinuity of the exchange-correlation (XC) functional.[3,6] As this contribution is positive and not small, the KS band gap underestimates severely the observed ones also for potentials believed to be close to the exact KS-DFT.[7–9]

The conventional solution to this so called band gap problem has been an empirical shift, often called as "scissor operation," to correct the too small band gap.[10] Tran and Blaha[11] published a different approach with semilocal model potential to evaluate band gaps of solids by fitting the potential, defined with parameters, to increase KS band gap to reproduce the experimental one. However, due to the Hohenberg-Kohn theorem,[1] there is only one KS potential which yields the correct density, and it has been shown that the accurate many-body perturbation-theory-based KS potential yields a KS gap, which in most cases is only little more than half of the experimental one.[6–8] The previous statements reflect our point of view, for we will consider these potentials as best available references and will compare our results accordingly.

The potential discontinuity at integer particle number is only an artifact of multiplicative KS potential and the proper quasiparticle picture such as nonlocal Hartree-Fock or nonlocal and energy-dependent GW (Ref. 12) directly yields the quasiparticle band gap as a one electron energy difference of highest occupied and lowest unoccupied levels. Thus, there are different approaches to obtain good quasiparticle band gaps, KS-DFT with a multiplicative potential and others which employ nonlocality, either spatial or temporal (energy dependence). The evaluation of the discontinuity for a multiplicative KS potential has been stated necessary and cumbersome[13] but in case of GLLB it is trivial.

A general formalism to obtain the KS potential for a given (not explicitly density dependent) energy functional is the optimized effective potential (OEP) method,[14,15] where the total-energy functional is minimized with respect to variations in a multiplicative XC potential. Correlation contributions can also be included,[16–18] but a common approach is so called exact-exchange OEP (EXX-OEP) formalism,[19] where the Hartree-Fock exchange energy functional is adopted as the first-order term of the adiabatic perturbation theory.[20]

Several approximations have been suggested for solving the complicated and computationally demanding OEP equations, such as common denominator approximation based on so called KLI (Ref. 21) and LHF (Ref. 22) potentials. The practical calculations for large systems, however, call for more robust approaches.

In this study we present one such alternative. We start with the computationally attractive GLLB potential by Gritsenko *et al.*,[23] which is a further approximation to KLI potential. The model includes the useful properties of the electron gas as well as a discontinuity on integer particle number. The GLLB potential is further modified by replacing the used energy density functional to another, more suitable for solids and adding correlation. This results in a potential which we call GLLB-SC (solid, correlation).

We have implemented our approach along with the GLLB within the projector augmented wave (PAW) method in the

real-space grid based GPAW code.[24] As a test set we consider the elemental semiconductors C, Si, and Ge, and compound semiconductors GaAs and AlAs. Furthermore, we study two wide gap insulators LiF and Ar. Except for Ge, the test set is chosen to match the available many-body perturbation-theory data.[6–8] We evaluate both the direct band gaps in high-symmetry points of the Brillouin zone and the fundamental indirect band gap where relevant. In each case the two contributions to the quasiparticle gap, the KS band gap and the discontinuity Δ_{xc} are given. We compare our data to the experimentally observed and to other calculated results, where available.

In Sec. II the basic concepts are defined and the Sham-Schlüter equation is briefly introduced. The GLLB model potential is introduced in Sec. III and extended to suit better for solids and band gap materials, in particular. In Sec. IV the discontinuity of GLLB potential is discussed. Section V gives some details about implementation to the GPAW code. Finally, the results are given in Sec. VI and conclusions in Sec. VII.

II. QUASIPARTICLE BAND GAP

The KS-DFT XC potential of an N-electron system is the functional derivative of the XC energy as

$$v_{xc}(\mathbf{r};N) = \left. \frac{\delta E_{xc}[n]}{\delta n(\mathbf{r})} \right|_N. \tag{1}$$

It is continuous with respect to the fractional number of electrons but at integer occupations J a discontinuity may emerge as

$$\Delta_{xc} = \Delta_{xc}(\mathbf{r}) = v_{xc}(\mathbf{r};J+\delta) - v_{xc}(\mathbf{r};J-\delta), \tag{2}$$

where the limits $\delta \rightarrow 0$ are implied. The discontinuity Δ_{xc} is a constant function of $\mathbf{r}$.[3]

Within the exact DFT, the quasiparticle band gap of an N-electron system, the difference of the ionization potential (I) and electron affinity (A), consists of two contributions[3,6]

$$E_g^{QP} = I - A = E[n_{N-1}] - 2E[n_N] + E[n_{N+1}] = E_g^{KS} + \Delta_{xc}, \tag{3}$$

where the first term $E_g^{KS} = \varepsilon_{N+1} - \varepsilon_N$ is the KS band gap and the second term is the derivative discontinuity.

First estimates for the derivative discontinuity on real material was given by Godby *et al.*,[9] who solved v_{xc} from the Sham-Schlüter equation[6]

$$0 = \int d\omega \int d2 \int d3 G_{KS}(\mathbf{r}_1,2;\omega),$$

$$\{\Sigma^{xc}(2,3;\omega) - v_{xc}^{KS}(\mathbf{r}_2)\delta(2-3)\}G(3,\mathbf{r}_1;\omega) \tag{4}$$

by linearization: the interacting Green's function G and G_{KS} were both replaced by the G_{LDA}. The resulting potential is expected to be close to true KS-DFT, thus, leading to the band gaps equally close. Therefore, we compare GLLB and GLLB-SC band gaps to those obtained by Godby *et al.*[8,9] for C, Si, GaAs, and AlAs. Later, Grüning *et al.*[7] evaluated using

similar methods for Si, LiF, and Ar. We refer to all these data as "True" KS values, later on.

III. GLLB EXCHANGE AND COULOMB CORRELATION

The exchange and correlation energy functional can be written in terms of coupling constant averaged pair correlation function $\bar{g}_{xc}$ (Refs. 23 and 25) and Coulomb kernel $v(\mathbf{r}_1,\mathbf{r}_2) = |\mathbf{r}_1 - \mathbf{r}_2|^{-1}$ as

$$E_{xc}[n] = \frac{1}{2} \int d\mathbf{r}_1 \int d\mathbf{r}_2 n(\mathbf{r}_1)n(\mathbf{r}_2)$$

$$\times v(\mathbf{r}_1,\mathbf{r}_2)[\bar{g}_{xc}(n)(\mathbf{r}_1,\mathbf{r}_2) - 1], \tag{5}$$

which leads to the exchange-correlation potential in Eq. (1) as[23,25]

$$v_{xc}(\mathbf{r}) = v_{scr}(\mathbf{r}) + v_{resp}(\mathbf{r}), \tag{6}$$

where the two contributions are

$$v_{scr}(\mathbf{r}_1) = \int d\mathbf{r}_2 n(\mathbf{r}_2)v(\mathbf{r}_1,\mathbf{r}_2)[\bar{g}_{xc}(n)(\mathbf{r}_1,\mathbf{r}_2) - 1] \tag{7}$$

and

$$v_{resp}(\mathbf{r}_1) = \frac{1}{2} \int d\mathbf{r}_2 \int d\mathbf{r}_3 n(\mathbf{r}_2)n(\mathbf{r}_3)$$

$$\times v(\mathbf{r}_2,\mathbf{r}_3)\frac{\delta \bar{g}_{xc}[n](\mathbf{r}_2,\mathbf{r}_3)}{\delta n(\mathbf{r}_1)}. \tag{8}$$

The screening part $v_{scr}(\mathbf{r})$ is the Coulombic potential of the XC hole, corresponding to the Slater potential in the exchange-only case. Thus, it has a smooth and attractive form. The response part $v_{resp}(\mathbf{r})$ arises from the pair correlation function response to the density variations. It is repulsive and short ranged. Next, these two parts will be approximated with the help of a GGA functional.

In the original GLLB approach[23] the B88 exchange functional was used because of the correct asymptotic behavior $(-1/r)$ and a parameter fit to atoms.[26] Obviously, these are important features for small finite systems. We choose a modification of PBE functional[27] for solids,[28] PBEsol, instead. It is the "state-of-the-art" density functional, to restore the response properties of local density approximation and the jellium surface energy. As we deal with the electronic structures of solids, the choice is natural. PBEsol is a generalized gradient approximation, consequently neglecting the nonlocal effects such as London dispersion forces.

In the further work,[25] the GLLB screening was completed with a correlation contribution from the energy density of Perdew and Wang.[29] In this work we write for the screening potential approximation

$$v_{scr}(\mathbf{r}) = 2\epsilon_{xc}^{(PBEsol)}(\mathbf{r}), \tag{9}$$

where $\epsilon_{xc}^{(PBEsol)}$ is the XC energy density.

The exchange response part is the central issue here, and therefore, it deserves a closer look. First, within the KLI approximation[21] the exchange response potential is written as

$$v_{\mathrm{resp}}(\mathbf{r}) = \sum_i^{\mathrm{occ}} w_i \frac{|\psi_i(\mathbf{r})|^2}{n(\mathbf{r})}, \tag{10}$$

where the coefficients w_i are chosen self-consistently as

$$w_i = \langle i | v_{\mathrm{x}}(\mathbf{r}) - \hat{V}_{\mathrm{x}}^{(\mathrm{HF})} | i \rangle, \tag{11}$$

where $\hat{V}_{\mathrm{x}}^{(\mathrm{HF})}$ is the computationally heavy Fock operator.

The corresponding approximate exchange response part of GLLB was formulated by Gritsenko *et al.*[23] using several physical arguments: exchange scaling relation, asymptotic behavior and fit to the homogeneous electron gas (HEG). This was carried out by formulation of a simple expression for the orbital dependent function w_i, Eq. (11), which only depends on KS eigenvalues.

Shift of the external potential by a constant should not have any physical effect, and thus, the function should depend on the differences of the eigenvalues, only. Therefore, the highest occupied eigenvalue ε_H is taken as a reference ε_r and we choose

$$w_i = f(\varepsilon_r - \varepsilon_i) \tag{12}$$

with the condition that $f(0) = 0$, as w_H should vanish.[21]

Furthermore, the exchange potential has the following scaling property:

$$v_{\mathrm{x}}[n_\lambda](\mathbf{r}) = \lambda v_{\mathrm{x}}[n](\lambda \mathbf{r}), \tag{13}$$

where $n_\lambda = \lambda^3 n(\lambda \mathbf{r})$ while the eigenvalues scale as

$$\varepsilon_i[n_\lambda] = \lambda^2 \varepsilon_i[n(\mathbf{r})]. \tag{14}$$

These imply that the function f should scale as

$$f[\lambda^2(\varepsilon_r - \varepsilon_i)] = \lambda f(\varepsilon_r - \varepsilon_i), \tag{15}$$

which is satisfied by the form

$$w_i = K_{\mathrm{x}} \sqrt{\varepsilon_r - \varepsilon_i}. \tag{16}$$

The response potential of the HEG is known and it is

$$v_{\mathrm{resp}} = \frac{k_{\mathrm{F}}}{2\pi}, \tag{17}$$

where the Fermi wave vector is $k_F = (3\pi^2 n)^{1/3}$. The corresponding response potential in this approach is

$$v_{\mathrm{resp}}^{\mathrm{HEG}} = \frac{V}{8\pi^3} \int_{|\mathbf{k}| < k_{\mathrm{F}}} d\mathbf{k} K_x \sqrt{\varepsilon_r - \varepsilon_{\mathbf{k}}}, \tag{18}$$

where the difference $\varepsilon_r - \varepsilon_k$ for the electron gas can be written as

$$\varepsilon_r - \varepsilon_k = (k_F^2/2 + v_{\mathrm{KS}}) - (k^2/2 + v_{\mathrm{KS}}). \tag{19}$$

Setting the right-hand sides of Eqs. (17) and (18) equal, evaluation of the integral yields the electron gas fitted prefactor

$$K_{\mathrm{x}} = \frac{8\sqrt{2}}{3\pi^2} \approx 0.382. \tag{20}$$

Gritsenko *et al.*[25] use this same functional form also for the correlation contribution in the response part and just fit

the relevant prefactor K_{c}, accordingly. We choose to use the GGA, again, and the same PBEsol as before, consistently. As $v_{\mathrm{c}} = v_{\mathrm{c,scr}} + v_{\mathrm{c,resp}}$, we simply write

$$v_{\mathrm{c,resp}}^{\mathrm{PBEsol}}(\mathbf{r}) = v_{\mathrm{c}}^{\mathrm{PBEsol}}(\mathbf{r}) - 2\epsilon_{\mathrm{c}}^{\mathrm{PBEsol}}(\mathbf{r}). \tag{21}$$

Thus, the total GLLB-SC potential can be finally written as

$$v_{\mathrm{GLLB-SC}}(\mathbf{r}) = 2\epsilon_{\mathrm{xc}}^{\mathrm{PBEsol}}(\mathbf{r}) + \sum_i^{\mathrm{occ}} K_{\mathrm{x}} \sqrt{\varepsilon_r - \varepsilon_i} \frac{|\psi_i(\mathbf{r})|^2}{n(\mathbf{r})}$$
$$+ v_{\mathrm{c,resp}}^{\mathrm{PBEsol}}(\mathbf{r}). \tag{22}$$

In summary, the above formulation is an orbital-dependent robust simplification of the KLI approximation[21] to the EXX-OEP (Ref. 19) following the guidelines of GLLB (Refs. 23 and 25) for the exchange. For correlation, our formulation adds PBEsol correlation,[28] which is consistent with the exchange screening part.

IV. DISCONTINUITY IN GLLB+SC

In this section, we discuss the discontinuity and its origin in response potential. For our GLLB-SC has only exchange discontinuity, the expression for the discontinuity is identical with that of GLLB. In both the potential is not a direct functional derivative of any XC energy functional, similarly to KLI (Ref. 21) and LHF (Ref. 22) approximations. However, due to the similar orbital dependence all these potentials exhibit the discontinuity on addition of an electron. In GLLB exchange response approximation, the discontinuity comes with the coefficients w_i in Eq. (12) from their straightforward dependence on the highest occupied electron state.

The reference energy ϵ_r for particle number N close to integer occupation J can be written as

$$\epsilon_r = \begin{cases} \epsilon_J & N \leq J \\ \epsilon_{J+1} & N > J \end{cases} \tag{23}$$

for when the occupation exceeds J, what was formerly lowest unoccupied molecular orbital becomes now the highest occupied. For the difference of the above and below limits of $v_{\mathrm{x}}(\mathbf{r})$ as $N \to J$, i.e., the discontinuity, one obtains straightforwardly

$$\Delta_{\mathrm{x,resp}}(\mathbf{r}) = \sum_i^N K_x(\sqrt{\varepsilon_{N+1} - \varepsilon_i} - \sqrt{\varepsilon_N - \varepsilon_i}) \frac{|\psi_i(\mathbf{r})|^2}{n(\mathbf{r})}. \tag{24}$$

As the above approximation is not a constant, but depends on the space coordinate, the wave functions would be affected. Therefore, to compare with our approach the first-order perturbation theory expression leading to the constant discontinuity should be evaluated as

$$\Delta_{\mathrm{x,resp}} = \langle \Psi_{N+1} | \Delta_{\mathrm{x,resp}}^{\mathrm{GLLB}} | \Psi_{N+1} \rangle. \tag{25}$$

By analyzing the term in Eq. (24) for different summation indices more closely, we note that it vanishes for $\epsilon_i \to -\infty$. Thus, the dominant contribution from this expression is from neighborhood of the Fermi energy as one would expect.

In addition, we wish to revise a connection between the Sham-Schlüter equation and several approximations to the

response potential such as in KLI or in GLLB. Using similar arguments as those in derivation of KLI, to simplify the Sham-Schlüter equation, Eq. (4), after cumbersome algebra Casida found an approximative solution to $v_{\mathrm{xc}}(\mathbf{r})$ in terms of the self-energy[17]

$$
v_{\mathrm{xc}}(\mathbf{r}) = \sum_i^N \frac{\mathrm{Re}\{\psi_i(\mathbf{r})\hat{\Sigma}^{\mathrm{xc}}(\epsilon_i)\psi_i(\mathbf{r})\}}{n(\mathbf{r})}
$$
$$
+ \sum_i^N \frac{\langle\psi_i|v_{\mathrm{xc}} - \hat{\Sigma}^{\mathrm{xc}}(\epsilon_i)|\psi_i\rangle|\psi_i(\mathbf{r})|^2}{n(\mathbf{r})}, \qquad (26)
$$

where the latter term is equivalent of the response part of KLI, if $\Sigma^{\mathrm{xc}} \approx \Sigma^{\mathrm{x}} = iG_{\mathrm{DFT}}v$, i.e., the x-only self-energy in OEP-EXX formalism, where v is the bare coulomb interaction. By relating Eqs. (11) and (16), the response potential of GLLB, and ours, turns out to be an approximation to the matrix element in Eq. (26) as

$$
\langle\Psi_i|v_{\mathrm{x}} - \hat{\Sigma}^{\mathrm{x}}(\epsilon_i)|\Psi_i\rangle \approx K_x\sqrt{\epsilon_r - \epsilon_i}. \qquad (27)
$$

V. IMPLEMENTATION

We have implemented the GLLB and GLLB-SC potentials to the grid-based projector augmented wave method code GPAW.[24] It is a pseudopotential free approach, which allows more accurate and controlled description of electronic structure than the conventional pseudopotential approximations. For PAW core electrons the frozen-core approximation is used.

The PAW method[30,31] is based on a linear transformation, which connects smooth wave functions (represented in coarse Cartesian grid in GPAW) to the accurate all-electron functions (represented using partial wave set within each augmentation sphere in GPAW). The transformation and the resulting one-particle equation are

$$
\hat{T}\widetilde{\Psi}(\mathbf{r}) = \Psi(\mathbf{r}), \qquad (28)
$$

$$
\hat{T}^\dagger\hat{H}\hat{T}\widetilde{\Psi}(\mathbf{r}) = E\hat{T}^\dagger\hat{T}\widetilde{\Psi}(\mathbf{r}). \qquad (29)
$$

Details of the transformation are given elsewhere.[24] Normal approach for deriving the PAW potential would to take the derivative of the total energy expression but since GLLB or GLLB-SC have no such expression we form the potential analogously by hand. The PAW potential consists of a smooth part, which can be chosen, "in principle," freely inside the augmentation sphere. To obtain sufficiently smooth potential, we choose the expression

$$
\widetilde{v}_{\mathrm{GLLB-SC}}(\mathbf{r}) = 2\epsilon_x^{\mathrm{PBEsol}}[\widetilde{n}(\mathbf{r}), |\nabla\widetilde{n}(\mathbf{r})|^2](\mathbf{r})
$$
$$
+ \sum_i^{\mathrm{val.}} K_G\sqrt{\epsilon_r - \epsilon_i}\frac{|\widetilde{\psi}_i(\mathbf{r})|^2}{\sum_i^{\mathrm{val.}}|\widetilde{\psi}_i(\mathbf{r})|^2}
$$
$$
+ v_c^{\mathrm{PBEsol}}[\widetilde{n}(\mathbf{r}), |\nabla\widetilde{n}(\mathbf{r})|^2](\mathbf{r}),
$$

which is clearly identical to all-electron GLLB-SC potential outside and smooth inside the augmentation spheres. The

GLLB potential is obtained similarly by replacing $\epsilon_x^{\mathrm{PBEsol}}$ by $\epsilon_x^{\mathrm{B88}}$ and omitting the correlation potential.

The smooth potential requires augmentation sphere corrections to obtain full-potential description and we calculate the total PAW Hamiltonian as

$$
\hat{v}_{\mathrm{xc}} = \widetilde{v}_{\mathrm{xc}}(\mathbf{r}) + \sum_a^{\mathrm{atoms}} \sum_{ij} |\widetilde{p}_i^a\rangle(\langle\phi_i^a|v_{\mathrm{xc}}^a(\mathbf{r})|\phi_j^a\rangle - \langle\widetilde{\phi}_i^a|\widetilde{v}_{\mathrm{xc}}^a(\mathbf{r})|\widetilde{\phi}_j^a\rangle)
$$
$$
\times\langle\widetilde{p}_j^a|, \qquad (30)
$$

where the spherical corrections are performed on a radial logarithmic grid and the smooth part on a sparse real-space grid. The $\widetilde{\phi}_i$ are the partial wave expansions used to generate pseudodensity within augmentation sphere and ϕ_i are corresponding all-electron partial waves. The partial waves $\widetilde{\phi}_i^a$ and projectors $\widetilde{p}_j^a$ are chosen biorthogonal, thus on infinite basis set limit $\Sigma_i|\widetilde{p}_i^a\rangle\langle\phi_i^a|$ and it's conjugate are identity operators within the augmentation sphere. The quantities v_{xc}^a and $\widetilde{v}_{\mathrm{xc}}^a$ are the radial all-electron xc potential and radial smooth xc potential correspondingly. They are constructed and integrated in 50 radial slices corresponding to Lebedev points in a unit sphere.

For core states, we use the response potential calculated for single atom. In addition, for calculating the discontinuity, we neglect the shift caused by the core states. This is justified for core states, for their contribution is small due to reasons described in Sec. IV.

Calculation of the potential scales as $O(N^2)$ with a small prefactor due to construction of the response potential, i.e., such as evaluation of the density from KS orbitals. Thus, the computation scales similarly as the normal local density functional potentials with a slightly larger prefactor arising mostly due to a larger number ($\approx 1.5\times$) of self-consistent-field iterations. In case of a general model potential, this issue is discussed further in Ref. 32.

VI. RESULTS AND DISCUSSION

To ensure convergence with respect to numerical parameters in calculations, a real space grid with about 0.11 Å spacing was used for the wave functions. We also used 17 $\times 17\times 17$ k points in the first Brillouin zone corresponding to the two atom unit cell to find the conduction-band minimum (CBM) state required for calculation of the discontinuity accurately. Note, that this is more than what is needed for convergence in the self-consistent electronic structure. Consequently, sufficient numerical accuracy in the obtained KS potential and $\Delta_{\mathrm{x,resp}}^{\mathrm{GLLB}}$ is guaranteed. Using these, the single-point band-structure calculations were performed using k points in high-symmetry points and directions in the first Brillouin zone.

Smooth and all-electron partial waves and the pseudoprojector functions were generated on default values provided with the GPAW code.[24] The frozen-core approximation was used. In case of Ga the 3d electrons were included into the frozen core to retain comparability to some earlier pseudopotential calculations but relaxation of the 3d electrons was tested and found to have only a minor effect on the band gap.
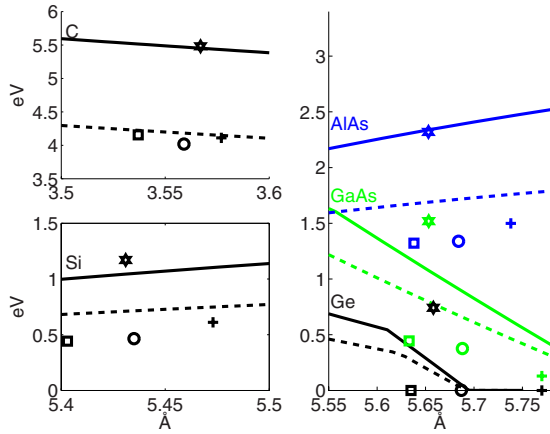
FIG. 1. (Color online) Fundamental, i.e., minimum, band gap (in eV) of five semiconductors as a function of the lattice constant. The KS gap (dashed curve) and the quasiparticle gaps (solid curve) from our GLLB-SC are shown. The LDA (square), PBE (plus), and PBEsol (circle) data are shown for their minimum energy lattice constants, respectively. Similarly, the experimental data is denoted by the star. For references, see Table I.

We do not have the total-energy functional to minimize in our approach for finding the crystal lattice constants of our test set semiconductor compounds, consistently. Therefore, we first consider the evaluated fundamental (minimum) band gaps as a function of the lattice constant in the range of LDA, GGA, and experimental gaps, shown in Fig. 1. The possible structural changes due to stress are not taken into account. Note, that our primary intention is not to evaluate band gap for materials under stress but to acknowledge the fact that the lattice constant has a large effect to the band gap. Therefore the band gap predicted using relaxed lattice constant depends not only on the XC potential but also on the energetic properties of XC functional (i.e., on the relaxed lattice constant itself).

Also, for comparison the LDA, PBEsol and experimental band gap lattice constant data is given. There, the usual tendency of LDA underestimating and GGA overestimating the experimentally found lattice constants is clearly seen. The PBEsol is seen to find a lattice constant in between these

two, and in average, closest to the experimental one. As GLLB-SC is based on PBEsol, it can be suggested to be used for evaluation of the lattice constants and other energetics for GLLB-SC, where relevant.

From our GLLB-SC approach the KS contribution and the total quasiparticle band gaps are shown. Lattice constant dependence is seen to be weak for C and Si but stronger for compound semiconductors and Ge. For GaAs and Ge the lattice constant dependence is strongest and match with experimental gaps is less good. The gap opens strongly with decreasing lattice constant. The success with Ge should be noticed, in particular, as the LDA and GGA do not open the gap, at all. The other cases show a good match with the experimental band gap in a large range of lattice constants.

From now on we restrict our analysis and discussion to the calculated band gaps using the following experimental lattice constants: C(3.567),[33] Si(5.431),[33] Ge(5.658),[33] GaAs(5.653),[33] AlAs(5.661),[34] LiF(4.024),[35] and Ar(5.260),[36] all in Å.

In Table I we list our calculated KS band gaps for LDA, GLLB, and GLLB-SC. These are to be compared with the band gap values obtained with potential from linearized Sham-Schlüter equations. Both GLLB and GLLB-SC yield KS band gaps close to these values. Comparing GLLB-SC and GLLB, GLLB-SC shifts the band gaps to the right direction with all materials except for Ar. Furthermore, we note that the obtained band gaps are much closer to expected KS values than the approach by Tran and Blaha[11] due to their choice of the fitting objective.

Furthermore, In Table I we list the calculated quasiparticle band gaps with added discontinuity using GLLB and GLLB-SC potentials. The GLLB and GLLB-SC use an electron gas based response potential resulting in a discontinuity which gives good quasiparticle band gaps to be compared with the GW and experimental results. We find this to be a remarkable result considering the fact that the quasiparticle band gaps evaluated from OEP-EXX potential are disastrously overestimated.[19]

In Fig. 2 we extend our analysis to all of the calculated direct KS band gaps of our test case semiconductors at the special symmetry points in the Brillouin zone. The discontinuities are shown as an additional bar on top. It should be

TABLE I. (a) The minimum KS band gaps/the fundamental band gap with discontinuity from GLLB exchange only and GLLB-SC calculations using the experimental lattice constants given in the text. (b) The KS-band gap based on Sham-Schlüter GW self-energy/GW quasiparticle band gap (Refs. 7 and 8). (c) Experimental values for C, Si, AlAs, and GaAs from Ref. 8 and references there in. For Ge we used 0 K value from Ref. 32. LiF and Ar values from Ref. 7. (d) Effect of spin-orbit splitting removed (see Ref. 8 for details). All units in eV.

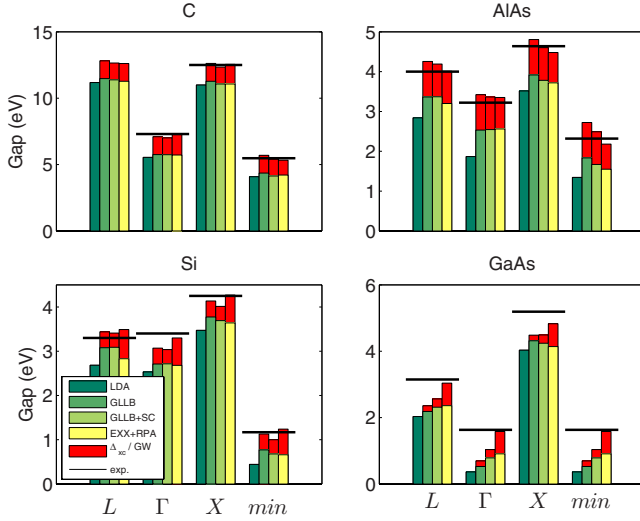| Compound	LDA	GLLB (a)	GLLB-SC (a)	KS/GW (b)	Expt. (c)
C	4.09	4.36/5.70	4.14/5.41	4.21/5.33	5.48
Si	0.44	0.77/1.13	0.68/1.00	0.66/1.24	1.17
Ge	0.00	0.00/0.00	0.21/0.27	NA	0.74
AlAs	1.34	1.83/2.72	1.67/2.49	1.55/2.18	2.32 (d)
GaAs	0.36	0.53/0.69	0.79/1.04	0.91/1.58	1.63 (d)
LiF	8.78	11.20/15.38	10.87/14.96	9.3/13.5	14.2
Ar	8.18	9.9/14.46	10.3/14.97	8.8/13.1	14.2

FIG. 2. (Color online) Kohn-Sham band gap (three leftmost, green) and the discontinuity (on top) contribution to the quasiparticle (total) gap from our LDA, GLLB exchange only, and GLLB-SC calculations. The True DFT KS gaps (rightmost, yellow) with the discontinuity from GW (top, red) are shown for comparison.

noted that Kohn-Sham DFT with added discontinuity guarantees only the fundamental band gap to be correct, for it is the only quantity which is a ground-state property in the band structure. However, we approximate also other band gaps by adding the calculated discontinuity also to them as shown in Fig. 2. Good match with the experiments is again seen, except for GaAs, as in Fig. 1 for the fundamental band gaps.

Next, we analyze the Kohn-Sham contribution to the band structure. First in Table II, we compare the KS band gaps of highest symmetry points of the first Brillouin zone for Si, LiF, and Ar crystals. LDA gives systematically the lowest gaps underestimating the true KS gaps while GLLB exchange only or GLLB-SC make a slight overestimation. However, the variation is small, and thus, not essential. The inaccuracy for comparing our projector augmented wave approach and the pseudopotential approach used for KS gaps is probably larger than the differences in band gaps.

Finally, we evaluate the Kohn-Sham band structures of the test compounds to analyze also the dispersion around
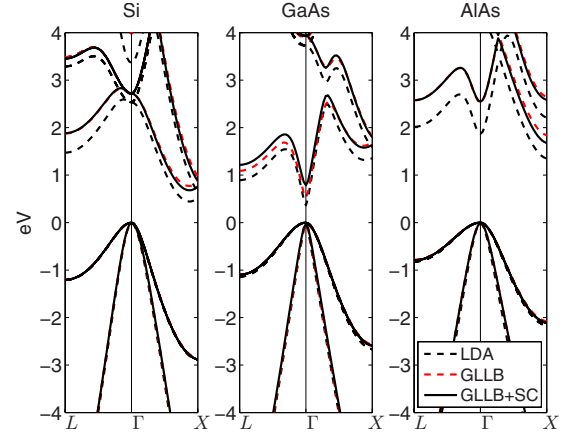

FIG. 3. (Color online) Calculated Kohn-Sham band structures (without discontinuity) of compounds Si, GaAs, and AlAs using LDA, GLLB, and GLLB-SC approaches.

valence and conduction bands. In Figs. 3 and 4 we compare LDA, GLLB, and GLLB-SC approaches. The constant discontinuity is removed for clarity.

Overlap of the bands from these approaches is close to perfect in the valence bands and below. There are no significant differences in the dispersion at the CBM or above, either. The small differences in the KS gap, see Table II, make a just rigid shift of the bands, only. This behavior seems to be similar in all considered cases.

We argue, that the full potential of model potentials is currently not used based on our positive experience for simple KS-eigenvalue-dependent GLLB exchange response potential for predicting the derivative discontinuity of the exchange-correlation energy functional. There are various local and global quantities which are fast to evaluate and could be used to construct a mapping between them and electron gas based expressions for potential. These include quantities such as the eigenvalues (or some other expectation values), wave functions and their gradients, etc. The simplest approach would be to make the response potential exact at electron gas limit by fitting the function f in Eq. (12) to $v_{c,resp}$ for electron gas. For the first hint, we related the GLLB response potential to the Casida's approximation to the Sham-Schlüter equation.

TABLE II. Kohn-Sham band gaps of high-symmetry points with respect to Γ point for Si, LiF, and Ar.

Comp.	Gap	LDA[a]	GLLB[a]	GLLB-SC[a]	True[b]	LDA[b]
Si	$\Gamma \rightarrow \Gamma$	2.53	2.71	2.72	2.6	2.6
	$\Gamma \rightarrow X$	0.58	0.91	0.81	0.6	0.7
	$\Gamma \rightarrow L$	1.47	1.88	1.88	1.5	1.5
LiF	$\Gamma \rightarrow \Gamma$	8.78	11.2	10.9	9.3	8.9
	$\Gamma \rightarrow X$	14.4	17.1	16.8	15.3	14.8
	$\Gamma \rightarrow L$	10.3	13.4	13.1	11.1	10.6
Ar	$\Gamma \rightarrow \Gamma$	8.18	9.9	10.3	8.8	8.2
	$\Gamma \rightarrow X$	10.9	12.3	12.7	11.4	10.6
	$\Gamma \rightarrow L$	11.1	12.5	12.8	11.5	11.0

[a]This work calculated using GPAW code (Ref. 24).
[b]EXX-RPA and LDA gaps calculated by Grüning *et al.* (Ref. 7). All units in eV.
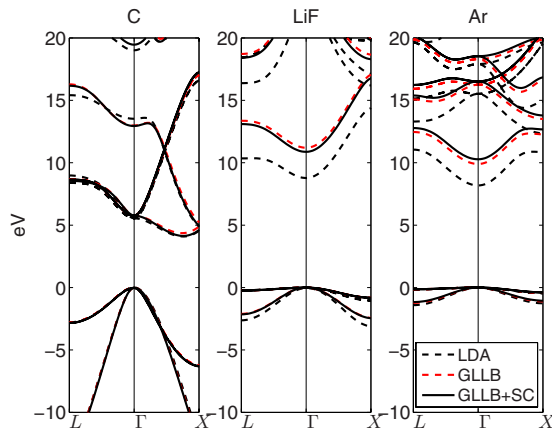
FIG. 4. (Color online) Calculated Kohn-Sham band structures (without discontinuity) of C, LiF, and Ar using LDA, GLLB, and GLLB-SC approaches.

VII. CONCLUSIONS

We have demonstrated how the derivative discontinuity at the integer occupation numbers can be included into a simple semilocal orbital-dependent exchange-correlation potential. Our approach, GLLB-SC, is based on the GLLB-type exchange of Gritsenko et al.[23] and PBEsol correlation,[28] where the former is responsible for bringing in the discontinuity in its "response part."

We have analyzed the roles of the two parts to the evaluated total quasiparticle band gap: Kohn-Sham gap and the discontinuity contribution. Both GLLB and GLLB-SC potentials contain only discontinuous exchange potential but nevertheless the agreement with experimental results is remarkable compared to computationally more expensive EXX approach, where the quasiparticle band gap is essentially same than the Hartree-Fock band gap.

The evaluated fundamental band gaps for our test set, typical semiconductors and dielectrics, match surprisingly well to the experimental data and to those from more sophisticated approaches. However, the computational efforts needed for GLLB-SC are about the same as for a typical GGA calculation, only. In short, we have demonstrated a computational approach to solve the "band gap problem" of semiconductors and shown that it gives close to correct band gaps.

[1] P. Hohenberg and W. Kohn, Phys. Rev. **136**, B864 (1964).

[2] W. Kohn and L. J. Sham, Phys. Rev. **140**, A1133 (1965).

[3] J. P. Perdew and M. Levy, Phys. Rev. Lett. **51**, 1884 (1983).

[4] A. Görling, Phys. Rev. A **54**, 3912 (1996).

[5] D. P. Chong, O. V. Gritsenko, and E. J. Baerends, J. Chem. Phys. **116**, 1760 (2002).

[6] L. J. Sham and M. Schlüter, Phys. Rev. Lett. **51**, 1888 (1983).

[7] M. Grüning, A. Marini, and A. Rubio, J. Chem. Phys. **124**, 154108 (2006).

[8] R. W. Godby, M. Schlüter, and L. J. Sham, Phys. Rev. B **36**, 6497 (1987).

[9] R. W. Godby, M. Schlüter, and L. J. Sham, Phys. Rev. Lett. **56**, 2415 (1986).

[10] Z. H. Levine and D. C. Allan, Phys. Rev. Lett. **63**, 1719 (1989).

[11] F. Tran and P. Blaha, Phys. Rev. Lett. **102**, 226401 (2009).

[12] L. Hedin, Phys. Rev. **139**, A796 (1965).

[13] M. Grüning, A. Marini, and A. Rubio, Phys. Rev. B **74**, 161103(R) (2006).

[14] J. D. Talman and W. F. Shadwick, Phys. Rev. A **14**, 36 (1976).

[15] R. T. Sharp and G. K. Horton, Phys. Rev. **90**, 317 (1953).

[16] T. Grabo and E. K. U. Gross, Chem. Phys. Lett. **240**, 141 (1995).

[17] M. E. Casida, Phys. Rev. A **51**, 2005 (1995).

[18] T. Kotani, J. Phys.: Condens. Matter **10**, 9241 (1998).

[19] M. Städele, J. A. Majewski, P. Vogl, and A. Görling, Phys. Rev. Lett. **79**, 2089 (1997).

[20] A. Görling and M. Levy, Phys. Rev. A **50**, 196 (1994).

[21] J. B. Krieger, Y. Li, and G. J. Iafrate, Phys. Rev. A **45**, 101 (1992).

[22] F. D. Sala and A. Görling, J. Chem. Phys. **115**, 5718 (2001).

[23] O. Gritsenko, R. van Leeuwen, E. van Lenthe, and E. J. Baerends, Phys. Rev. A **51**, 1944 (1995).

[24] J. J. Mortensen, L. B. Hansen, and K. W. Jacobsen, Phys. Rev. B **71**, 035109 (2005).

[25] O. Gritsenko, R. van Leeuwen, and E. J. Baerends, Int. J. Quantum Chem. **61**, 231 (1997).

[26] A. D. Becke, Phys. Rev. A **38**, 3098 (1988).

[27] J. P. Perdew, K. Burke, and M. Ernzerhof, Phys. Rev. Lett. **77**, 3865 (1996).

[28] J. P. Perdew, A. Ruzsinszky, G. I. Csonka, O. A. Vydrov, G. E. Scuseria, L. A. Constantin, X. Zhou, and K. Burke, Phys. Rev. Lett. **100**, 136406 (2008).

[29] Y. Wang and J. P. Perdew, Phys. Rev. B **44**, 13298 (1991).

[30] P. E. Blöchl, Phys. Rev. B **50**, 17953 (1994).

[31] P. E. Blöchl, C. J. Först, and J. Schimpl, Bull. Mater. Sci. **26**, 33 (2003).

[32] A. P. Gaiduk and V. N. Staroverov, J. Chem. Phys. **131**, 044107 (2009).

[33] M. Levinshtein, S. Rumyantsev, and M. Shur, *Handbook Series on Semiconductor Parameters* (World Scientific, Singapore, 1996), Vol. 1.

[34] M. Levinshtein, S. Rumyantsev, and M. Shur, *Handbook Series on Semiconductor Parameters* (World Scientific, Singapore, 1999), Vol. 2.

[35] H.-J. Ullrich, A. Uhlig, G. Geise, H. Horn, and H. Waltinger, Mikrochim. Acta **107**, 283 (1992).

[36] R. J. Magyar, A. Fleszar, and E. K. U. Gross, Phys. Rev. B **69**, 045111 (2004).